

Radiative corrections to inverse muon decay for accelerator neutrinos

OLEKSANDR TOMALAK ^{*1}, KAUSHIK BORAH^{2,3}, RICHARD J. HILL^{2,3},
 KEVIN S. MCFARLAND⁴, AND DANIEL RUTERBORIES⁴

¹*Theoretical Division, Los Alamos National Laboratory, Los Alamos, NM 87545, USA*

²*University of Kentucky, Department of Physics and Astronomy, Lexington, KY 40506, USA*

³*Fermilab, Theoretical Physics Department, Batavia, IL 60510, USA*

⁴*University of Rochester, Department of Physics and Astronomy, Rochester, NY 14627, USA*

November 30, 2022

Inverse muon decay ($\nu_\mu e^- \rightarrow \nu_e \mu^-$) is a promising tool to constrain neutrino fluxes with energies $E_\nu \geq 10.9$ GeV. Radiative corrections introduce percent-level distortions to energy spectra of outgoing muons and depend on experimental details. In this paper, we generalize the framework of radiative corrections in muon decay to the scattering processes $\nu_\mu e^- \rightarrow \nu_e \mu^-$ and $\bar{\nu}_e e^- \rightarrow \bar{\nu}_\mu \mu^-$. We evaluate virtual and real $\mathcal{O}(\alpha)$ contributions and present the muon energy spectrum and double-differential distributions in muon energy and muon scattering angle, and in muon energy and photon energy. We discuss how radiative corrections modify experimentally interesting distributions.

Contents

1	Introduction	2
2	Inverse muon decay at tree level	2
3	Virtual corrections	3
4	Real radiation	4
4.1	Soft-photon Bremsstrahlung	4
4.2	Contribution of hard photons	5
5	Muon energy spectrum and integrated cross section	6
6	Distortion of experimentally-accessed distributions	8
7	Conclusions and Outlook	11
A	Triple-differential distribution	14
B	Double-differential distribution in muon energy and muon angle	15
	References	15

*tomalak@lanl.gov

1 Introduction

Scattering of neutrino beams from atomic electrons provides us a “Standard Candle” for constraints on the neutrino fluxes at accelerator-based experiments. For example, the MINERvA experiment exploits the elastic scattering channel $\nu_\ell e^- \rightarrow \nu_\ell e^-$ [1–4] for the normalization of all (anti)neutrino-nucleus cross-section measurements. Another pure-leptonic process, inverse muon decay $\nu_\mu e^- \rightarrow \nu_e \mu^-$ and $\bar{\nu}_e e^- \rightarrow \bar{\nu}_\mu \mu^-$, requires (anti)neutrinos to be sufficiently energetic to produce the massive muon in the final state. The incoming energy should be larger than 10.9 GeV, which is slightly above the main region of modern artificial (anti)neutrino fluxes. Moreover, such high-energy tails are a very uncertain part of the (anti)neutrino beam [2] due to less-known hadroproduction cross sections for forward-going mesons in the direction of the proton beam. Recently, high-energy tails of the muon component in the incoming neutrino beam were also successfully constrained with the inverse muon decay (IMD) reaction $\nu_\mu e^- \rightarrow \nu_e \mu^-$ by the MINERvA experiment [5]. According to the study in Ref. [6], the future DUNE experiment [7] will have tens of thousands of elastic neutrino-electron scattering events and more than a few thousand inverse muon decay events. Consequently, both reactions will be accessed at the percent level, and radiative corrections become crucial for the correct interpretation of experimental measurements [8, 9].

A comprehensive theoretical study of radiative corrections and various final-state distributions in elastic neutrino-electron scattering with error analysis was recently presented in Ref. [10] and compared to all previous calculations discussed in Refs. [11–30]. Radiative corrections to the inverse muon decay were discussed in the ultrarelativistic limit in Ref. [14] and subsequently evaluated in Ref. [31]. Before the above-mentioned measurements by the MINERvA Collaboration, IMD results from the CHARM-II Collaboration [32, 33] have confirmed predictions of the Standard Model of particle physics.

In this paper, we generalize the recently-developed framework of radiative corrections to (anti)neutrino energy spectra in the muon decay $\mu^- \rightarrow e^- \nu_e \bar{\nu}_\mu$ [34] to the cross channel of IMD. Virtual corrections are described by the same form factors, while for the contribution of hard photons, we perform a straightforward integration by a technique of Refs. [9–11, 34, 35]. The most relevant observable in the experiment is the muon energy spectrum with or without restrictions on the energy of the radiated real photon. The muon is scattered primarily in the forward direction. Although experimental resolution does not allow a precise determination of the muon scattering angle, the muon angular distribution can potentially provide better selection criteria for IMD events. We compare our results for the muon energy spectrum with the Bardin-Dokuchaeva calculation [31] and provide expressions for double-differential distributions in muon energy and muon scattering angle as well as in muon energy and photon energy. We discuss how radiative corrections modify the experimentally-sensitive distributions from Ref. [5].

The paper is organized as follows. In Section 2, we discuss the IMD reaction at tree level. We provide virtual radiative corrections in Section 3 and describe the evaluation of real contributions in Section 4. We combine these calculations to obtain the resulting muon-energy spectrum at $\mathcal{O}(\alpha)$ precision in Section 5, where we also present the total cross section, double-differential distribution in muon energy and muon scattering angle, double-differential distribution in muon energy and photon energy, and triple-differential distribution in muon energy, muon scattering angle, and photon energy for the first time. In the following Section 6, we discuss distortions of experimentally-accessed distributions due to $\mathcal{O}(\alpha)$ radiative corrections. We finish with conclusions and outlook in Section 7. We provide new expressions for the triple-differential distribution in muon energy, muon scattering angle and photon energy, and double-differential distribution in muon energy and muon scattering angle in Appendices A and B, respectively.

2 Inverse muon decay at tree level

Consider muon production on atomic electrons by a neutrino beam, $\nu_\mu(k_{\nu_\mu}) e^-(p_e) \rightarrow \nu_e(k_{\nu_e}) \mu^-(p_\mu)$ [or $\bar{\nu}_e(k_{\bar{\nu}_e}) e^-(p_e) \rightarrow \bar{\nu}_\mu(k_{\bar{\nu}_\mu}) \mu^-(p_\mu)$]. This process is governed by the low-energy effective four-fermion

interaction with scale-independent Fermi coupling constant G_F [34, 36–40]

$$\mathcal{L}_{\text{eff}} = -2\sqrt{2}G_F\bar{\nu}_e\gamma^\lambda P_L\nu_\mu\bar{\mu}\gamma_\lambda P_L e + \text{h.c.} \quad (1)$$

The reaction is kinematically allowed only for sufficiently high energies of the incoming neutrino $E_{\nu_\mu}, E_{\bar{\nu}_e} \geq E_\nu^{\text{thr}}$, where

$$E_\nu^{\text{thr}} = \frac{m_\mu^2 - m_e^2}{2m_e}. \quad (2)$$

In radiation-free kinematics, the muon goes predominantly in the forward direction with a scattering angle θ_μ :

$$\cos\theta_\mu = \frac{2(E_\nu E_\mu + m_e E_\mu - m_e E_\nu) - m_\mu^2 - m_e^2}{2E_\nu\sqrt{E_\mu^2 - m_\mu^2}}. \quad (3)$$

The corresponding cone size increases with incoming (anti)neutrino energy. For example, the scattering within 0.2° is allowed only for the incoming (anti)neutrino energy $E_\nu \gtrsim 38$ GeV.

The differential cross section w.r.t. the muon energy E_μ , as a function of the incoming neutrino energy E_ν , is given by

$$\frac{d\sigma_{\text{LO}}(\nu_\mu e^- \rightarrow \nu_e \mu^-, \bar{\nu}_e e^- \rightarrow \bar{\nu}_\mu \mu^-)}{dE_\mu} = \frac{|\text{T}_{\text{LO}}|^2}{32\pi m_e E_\nu^2}, \quad (4)$$

where the squared matrix element at leading order is $|\text{T}_{\text{LO}}|^2 = 64G_F^2 p_\mu \cdot k_{\nu_e} p_e \cdot k_{\nu_\mu}$ in $\nu_\mu(k_{\nu_\mu}) e^-(p_e) \rightarrow \nu_e(k_{\nu_e}) \mu^-(p_\mu)$ and $|\text{T}_{\text{LO}}|^2 = 64G_F^2 p_\mu \cdot k_{\bar{\nu}_e} p_e \cdot k_{\bar{\nu}_\mu}$ in $\bar{\nu}_e(k_{\bar{\nu}_e}) e^-(p_e) \rightarrow \bar{\nu}_\mu(k_{\bar{\nu}_\mu}) \mu^-(p_\mu)$. Integration of this distribution over the kinematically allowed range of muon energies,

$$E_\mu^{\text{min}} = \frac{m_\mu^2 + m_e^2}{2m_e} \leq E_\mu \leq \frac{(E_\nu + \frac{m_e}{2})^2 + \frac{m_\mu^2}{4}}{E_\nu + \frac{m_e}{2}} = E_\mu^{\text{max}}, \quad (5)$$

results in the following total cross sections [31]:

$$\sigma_{\text{LO}}(\nu_\mu e^- \rightarrow \nu_e \mu^-) = \frac{2G_F^2 m_e (E_\mu^{\text{max}} - E_\mu^{\text{min}})}{\pi} \frac{E_{\nu_\mu} - E_\nu^{\text{thr}}}{E_{\nu_\mu}}, \quad (6)$$

$$\begin{aligned} \sigma_{\text{LO}}(\bar{\nu}_e e^- \rightarrow \bar{\nu}_\mu \mu^-) = & \frac{2G_F^2 m_e (E_\mu^{\text{max}} - E_\mu^{\text{min}})}{\pi} \left(\frac{(E_\mu^{\text{max}})^2 + E_\mu^{\text{max}} E_\mu^{\text{min}} + (E_\mu^{\text{min}})^2}{3E_{\bar{\nu}_e}^2} + \frac{E_{\bar{\nu}_e} + m_e}{E_{\bar{\nu}_e}} \frac{E_{\bar{\nu}_e} + E_\mu^{\text{min}}}{E_{\bar{\nu}_e}} \right. \\ & \left. - \frac{E_{\bar{\nu}_e} + E_\mu^{\text{min}} - \frac{E_\nu^{\text{thr}}}{2}}{E_{\bar{\nu}_e}} \frac{E_\mu^{\text{max}} + E_\mu^{\text{min}}}{E_{\bar{\nu}_e}} \right). \end{aligned} \quad (7)$$

In the following Sections, we include virtual and real radiative corrections to the inverse muon decay cross section.

3 Virtual corrections

To evaluate virtual contributions, it is convenient to express vertex corrections as a deviation of the charged-lepton current $(\delta J^L)^\nu$ from the tree-level expression $(J^L)^\nu = \bar{\mu}(p_\mu) \gamma^\nu P_L e(p_e)$ as

$$(\delta J^L)^\nu = e^2 \int \frac{d^d L}{(2\pi)^d} \frac{\bar{\mu}(p_\mu) \gamma^\lambda (\not{p}_\mu - \not{L} + m_\mu) \gamma^\nu P_L (\not{p}_e - \not{L} + m_e) \gamma^\rho e(p_e)}{[(p_\mu - L)^2 - m_\mu^2][(p_e - L)^2 - m_e^2]} \Pi_{\lambda\rho}(L), \quad (8)$$

with the momentum-space photon propagator $\Pi^{\mu\nu}$:

$$\Pi^{\mu\nu}(L) = \frac{i}{L^2 - \lambda^2} \left[-g^{\mu\nu} + (1 - \xi_\gamma) \frac{L^\mu L^\nu}{L^2 - a\xi_\gamma \lambda^2} \right], \quad (9)$$

where the photon mass λ regulates the infrared divergence, ξ_γ is the photon gauge-fixing parameter, and a is an arbitrary constant. The corresponding field renormalization factors for the external charged leptons are evaluated from the one-loop self energies in the $\overline{\text{MS}}$ renormalization scheme as [10, 41–43]

$$Z_\ell = 1 - \frac{\alpha}{4\pi} \frac{\xi_\gamma}{\varepsilon} - \frac{\alpha}{4\pi} \left(\ln \frac{\mu^2}{m_\ell^2} + 2 \ln \frac{\lambda^2}{m_\ell^2} + 4 \right) + \frac{\alpha}{4\pi} (1 - \xi_\gamma) \left(\ln \frac{\mu^2}{\lambda^2} + 1 + \frac{a\xi_\gamma \ln a\xi_\gamma}{1 - a\xi_\gamma} \right), \quad (10)$$

with the renormalization scale in dimensional regularization μ , where the number of dimensions is $d = 4 - 2\varepsilon$. Neglecting Lorentz structures whose contractions with the (anti)neutrino current vanish at $m_\nu = 0$ and denoting the ratio of lepton masses as $r = m_e/m_\mu$, the resulting correction to the charged lepton current is expressed as

$$\left(\sqrt{Z_e Z_\mu} - 1 \right) (J^L)^\nu + (\delta J^L)^\nu = \frac{\alpha}{2\pi} \bar{\mu}(p_\mu) \left(g_M \gamma^\nu - f_2 \frac{p_\mu^\nu + r p_e^\nu}{2m_\mu r^2} - g_M^5 \gamma^\nu \gamma_5 + f_2^5 \frac{p_\mu^\nu - r p_e^\nu}{2m_\mu r^2} \gamma_5 \right) e(p_e), \quad (11)$$

where the form factors g_M , g_M^5 , f_2 , and f_2^5 are [34]:

$$\begin{aligned} g_M^{(5)}(\eta, r, \beta) = & -1 + \frac{1}{\beta} \left(\frac{1}{2} \left(2\beta - \ln \frac{1+\beta}{1-\beta} \right) \ln \frac{2m_e}{\lambda} + \frac{1}{2} \ln \frac{1+\beta}{1-\beta} \ln \frac{1+\beta}{\beta} - \ln \frac{r\sqrt{1-\beta} - \sqrt{1+\beta}}{r\sqrt{1+\beta} - \sqrt{1-\beta}} \frac{\ln r}{2} \right. \\ & + \frac{3}{8} \ln \frac{1+\beta}{1-\beta} + \frac{\sqrt{1-\beta^2}}{8\eta} \ln \frac{1+\beta}{1-\beta} + \frac{1}{4} \ln \frac{1+\beta}{1-\beta} \ln \frac{2r - (1+r^2)\sqrt{1-\beta^2}}{1-\beta} + \frac{\pi^2}{12} \\ & + \frac{1}{2} \text{Li}_2 \frac{1-\beta}{1+\beta} - \frac{1}{2} \text{Li}_2 \left(\frac{\sqrt{1-\beta}}{\sqrt{1+\beta}} r \right) - \frac{1}{2} \text{Li}_2 \left(\frac{\sqrt{1-\beta}}{\sqrt{1+\beta}} \frac{1}{r} \right) - \frac{5}{16} \ln^2 \frac{1+\beta}{1-\beta} - \frac{1}{4} \ln^2 r \Big) \\ & + \frac{\sqrt{1-\beta^2}}{8\beta} \frac{(r+\eta)^2 (1-\eta\sqrt{1-\beta^2})}{2r - (1+r^2)\sqrt{1-\beta^2}} \ln \frac{1+\beta}{1-\beta} - \frac{12r - (7+5r^2)\sqrt{1-\beta^2}}{2r - (1+r^2)\sqrt{1-\beta^2}} \frac{\ln r}{4} - \ln \frac{2}{r}, \quad (12) \end{aligned}$$

$$f_2^{(5)}(\eta, r, \beta) = \frac{r^2 \sqrt{1-\beta^2}}{2} \frac{1 - \eta\sqrt{1-\beta^2}}{\beta (2r - (1+r^2)\sqrt{1-\beta^2})} \ln \frac{1+\beta}{1-\beta} - \frac{r-\eta}{r+\eta} \frac{r^2 \sqrt{1-\beta^2}}{2r - (1+r^2)\sqrt{1-\beta^2}} \ln r. \quad (13)$$

Here β is the velocity of the muon in the electron rest frame, $\eta = 1$ for the form factors g_M , f_2 and $\eta = -1$ for the form factors g_M^5 , f_2^5 .

4 Real radiation

Inverse muon decay with single photon emission is described by the Bremsstrahlung contribution $T^{1\gamma}$:

$$T^{1\gamma} = -2\sqrt{2}G_{\text{Fie}} \bar{\nu}_e \gamma^\mu P_L \nu_\mu \left[\left(\frac{p_\mu^\nu}{p_\mu \cdot k_\gamma} - \frac{p_e^\nu}{p_e \cdot k_\gamma} \right) \bar{\mu} \gamma_\mu P_L e + \frac{1}{2} \bar{\mu} \left(\frac{\gamma^\nu \not{k}_\gamma \gamma_\mu}{p_\mu \cdot k_\gamma} + \frac{\gamma_\mu \not{k}_\gamma \gamma^\nu}{p_e \cdot k_\gamma} \right) P_L e \right] \varepsilon_\nu^*, \quad (14)$$

with the photon polarization four-vector ε_ν^* . Let us consider separately the cases of soft and hard photon emission.

4.1 Soft-photon Bremsstrahlung

The inverse muon decay with radiation of photons of arbitrary small energy cannot be experimentally distinguished from the decay without radiation. All events with photons below some energy cutoff $k_\gamma \leq$

ΔE (in the electron rest frame) must be included in measured observables. The corresponding scattering cross section factorizes in terms of the tree-level result of Eqs. (6) and (7) as

$$\sigma(\nu_\mu e^- \rightarrow \nu_e \mu^- \gamma, \bar{\nu}_e e^- \rightarrow \bar{\nu}_\mu \mu^- \gamma; k_\gamma \leq \Delta E) = \frac{\alpha}{\pi} \delta_s(\Delta E) \sigma_{\text{LO}}(\nu_\mu e^- \rightarrow \nu_e \mu^-, \bar{\nu}_e e^- \rightarrow \bar{\nu}_\mu \mu^-), \quad (15)$$

with the universal correction $\delta_s(\Delta E)$ [10, 14, 18, 26, 44]:

$$\delta_s(\Delta E) = \frac{1}{\beta} \left(\text{Li}_2 \frac{1-\beta}{1+\beta} - \frac{\pi^2}{6} \right) - \frac{2}{\beta} \left(\beta - \frac{1}{2} \ln \frac{1+\beta}{1-\beta} \right) \ln \frac{2\Delta E}{\lambda} + \frac{1}{2\beta} \ln \frac{1+\beta}{1-\beta} \left(1 + \ln \frac{\beta^{-2} \sqrt{1-\beta^2}}{4(1+\beta)^{-1}} \right) + 1. \quad (16)$$

This region of the phase space with low-energy photons cancels the infrared-divergent contributions from virtual diagrams. As a result, soft and virtual contributions multiply the tree-level cross sections of Eqs. (6) and (7) with infrared-finite factor, i.e., independent of the fictitious photon mass λ [45–48], as

$$\begin{aligned} \frac{\sigma(\nu_\mu e^- \rightarrow \nu_e \mu^-) + \sigma(\nu_\mu e^- \rightarrow \nu_e \mu^- \gamma (k_\gamma \leq \Delta E))}{\sigma_{\text{LO}}(\nu_\mu e^- \rightarrow \nu_e \mu^-)} &= 1 + \frac{\alpha}{\pi} \left\{ g_M + g_M^5 + \delta_s(\Delta E) \right. \\ &+ \left. \frac{r m_\mu^2}{4} \frac{(p_\mu - p_e)^2}{p_\mu \cdot k_{\nu_e} p_e \cdot k_{\nu_\mu}} (g_M - g_M^5) - \left(\frac{r^2 m_\mu^2}{4} \frac{(p_\mu - p_e)^2}{p_\mu \cdot k_{\nu_e} p_e \cdot k_{\nu_\mu}} + \frac{p_e \cdot k_{\nu_e}}{p_\mu \cdot k_{\nu_e}} \right) \left[\left(\frac{1+r}{2r} \right)^2 f_2 + \left(\frac{1-r}{2r} \right)^2 f_2^5 \right] \right\}, \end{aligned} \quad (17)$$

where we can obtain the contributions in the $\bar{\nu}_e e^- \rightarrow \bar{\nu}_\mu \mu^-$ reaction by replacing the momenta of neutrinos with the momenta of antineutrinos.

4.2 Contribution of hard photons

Here we evaluate the contribution of photons above the energy cutoff $k_\gamma \geq \Delta E$ to the muon energy spectrum. Squaring the matrix element of Eq. (14) for the inverse muon decay $\nu_\mu e^- \rightarrow \nu_e \mu^-$, we obtain the result in terms of Lorentz invariants as

$$\begin{aligned} \frac{|\mathbb{T}^{1\gamma}|^2}{e^2 |\mathbb{T}_{\text{LO}}|^2} &= - \left(\frac{p_\mu}{p_\mu \cdot k_\gamma} - \frac{p_e}{p_e \cdot k_\gamma} \right)^2 + \frac{p_\mu \cdot p_e}{p_e \cdot k_\gamma p_\mu \cdot k_\gamma} \left(\frac{k_{\nu_e} \cdot k_\gamma}{k_{\nu_e} \cdot p_\mu} - \frac{k_{\nu_\mu} \cdot k_\gamma}{k_{\nu_\mu} \cdot p_e} \right) + \frac{k_{\nu_\mu} \cdot k_\gamma}{p_e \cdot k_{\nu_\mu} p_e \cdot k_\gamma} - \frac{p_e \cdot k_{\nu_e}}{p_\mu \cdot k_{\nu_e} p_e \cdot k_\gamma} \\ &+ \frac{1}{p_\mu \cdot k_\gamma} - \frac{1}{p_e \cdot k_\gamma} + \frac{k_{\nu_e} \cdot k_\gamma}{p_\mu \cdot k_{\nu_e} p_\mu \cdot k_\gamma} + \frac{p_\mu \cdot k_{\nu_\mu}}{p_e \cdot k_{\nu_\mu} p_\mu \cdot k_\gamma} + \frac{k_{\nu_\mu} \cdot k_\gamma}{(p_e \cdot k_\gamma)^2} \frac{m_e^2}{p_e \cdot k_{\nu_\mu}} - \frac{k_{\nu_e} \cdot k_\gamma}{(p_\mu \cdot k_\gamma)^2} \frac{m_\mu^2}{p_\mu \cdot k_{\nu_e}}, \end{aligned} \quad (18)$$

while the result for $\bar{\nu}_e e^- \rightarrow \bar{\nu}_\mu \mu^-$ is given by the replacement of neutrino momenta by corresponding antineutrino momenta.

We perform the integration following the technique that was introduced in [11] and further developed in [9, 10, 34, 35]. For the inverse muon decay, the implementation is slightly more involved by having two mass scales: the electron mass and the muon mass.

First, we introduce the four-vector l : $l = p_e + k_\nu - p_\mu = (l_0, \vec{f})$. Working in the rest frame of atomic electrons, we have for the components of l :

$$l_0 = m_e + E_\nu - E_\mu, \quad (19)$$

$$f^2 = |\vec{f}|^2 = E_\nu^2 + \beta^2 E_\mu^2 - 2\beta E_\nu E_\mu \cos \theta_\mu. \quad (20)$$

Accounting for the conservation of energy and momentum, we obtain

$$l^2 = 2k_\gamma (l_0 - f \cos \gamma), \quad (21)$$

where γ denotes the angle between the photon direction and the vector \vec{f} . Using energy and momentum conservation to perform the integration over the final-state neutrino momentum components and the photon energy, we obtain the muon energy spectrum as

$$\frac{d\sigma^{1\gamma}}{dE_\mu} = \int \frac{|\mathbf{T}^{1\gamma}|^2}{256\pi^4 m_e} \frac{k_\gamma^2 f d f d\Omega_{k_\gamma}}{E_\nu^2 (l_0^2 - f^2)}. \quad (22)$$

It is convenient to split the phase space into two regions with distinct ranges of integration. There are no restrictions on the photon phase space in the region I: $l^2 \geq 2\Delta E (l_0 - f \cos \gamma)$. In this region, the range of kinematic variables is given by

$$m_e + \frac{2(\Delta E)^2}{m_e - 2\Delta E} + \frac{\frac{m_\mu^2 - m_e^2}{2}}{m_e - 2\Delta E} \leq E_\mu \leq m_e + \frac{2(E_\nu - \Delta E)^2}{m_e + 2(E_\nu - \Delta E)} + \frac{\frac{m_\mu^2 - m_e^2}{2}}{m_e + 2(E_\nu - \Delta E)}, \quad (23)$$

$$|E_\nu - \beta E_\mu| \leq f \leq l_0 - 2\Delta E, \quad (24)$$

$$\frac{l_0 - f}{2} \leq k_\gamma \leq \frac{l_0 + f}{2}. \quad (25)$$

In the complementary region II: $l^2 \leq 2\Delta E (l_0 - f \cos \gamma)$ that is close to the kinematics of the radiation-free process, the angle between the photon momentum and the vector \vec{f} is restricted as

$$\cos \gamma \geq \frac{1}{f} \left(l_0 - \frac{l^2}{2\Delta E} \right). \quad (26)$$

This region contributes a factorizable contribution δ_{II} , which adds linearly to $\delta_s(\Delta E)$ of Eq. (17) [10]:

$$\begin{aligned} \delta_{\text{II}} = & \frac{1}{\beta} \left(\left(\frac{1}{2} + \ln \frac{\rho(1 + \cos \delta_0)}{4\beta} \right) \ln \frac{1 - \beta}{1 + \beta} - \text{Li}_2 \frac{1 - \beta}{1 + \beta} - \text{Li}_2 \frac{\cos \delta_0 - 1}{\cos \delta_0 + 1} + \text{Li}_2 \left(\frac{\cos \delta_0 - 1}{\cos \delta_0 + 1} \frac{1 + \beta}{1 - \beta} \right) + \frac{\pi^2}{6} \right) \\ & + \ln \frac{1 - \beta \cos \delta_0}{\rho} - 1, \end{aligned} \quad (27)$$

where the angle δ_0 is given by

$$\cos \delta_0 = \frac{E_\nu^2 - \beta^2 E_\mu^2 - l_0^2}{2\beta E_\mu l_0}, \quad (28)$$

and $\rho = \sqrt{1 - \beta^2}$. Only the first term from Eq. (18) contributes in this region. The same term generates the ΔE -dependence after integrating over region I. For the muon energy spectrum including both soft and hard photons, this dependence cancels with the contribution of soft photons from Eq. (15). For other terms, we can safely set $\Delta E = 0$ starting from Eq. (18).

5 Muon energy spectrum and integrated cross section

Adding virtual and real corrections, we obtain the ΔE - and λ -independent result for the muon energy spectrum in the inverse muon decay $\nu_\mu e^- \rightarrow \nu_e \mu^-$ with photons of arbitrarily large energy allowed by kinematics. In the limit $E_\nu \gg m_e$ (i.e., neglecting order m_e/E_ν power corrections) our results are in

agreement with the calculation of Bardin and Dokuchaeva [31]:

$$\begin{aligned}
\frac{d\sigma}{dE_\mu} &= \frac{d\sigma_{\text{LO}}}{dE_\mu} + \frac{2G_{\text{F}}^2 m_e \alpha}{\pi} \frac{\alpha}{\pi} \left[\frac{1+3x}{2} \left(\text{Li}_2 \frac{1-\frac{x}{y}}{1-x} - \text{Li}_2 \frac{y-x}{1-x} - \ln \frac{y}{x} \ln \frac{y-x}{1-x} \right) \right. \\
&+ (1-x) \left(\left(\ln \frac{y^2}{xr_e} - 2 \right) \ln \frac{y-x}{y} + \ln \frac{y}{x} \ln(1-y) - \text{Li}_2 x + \text{Li}_2 y + \text{Li}_2 \frac{x-y}{1-y} + \frac{3}{2} (1-x) \ln(1-x) \right) \\
&- \frac{7x^3}{36} y^{-3} + \frac{x^2}{12} \left(1 + \frac{7x}{2} \right) y^{-2} + \left(-\frac{7x}{12} - \frac{x^2}{2} - \frac{x^3}{6} \right) y^{-1} - \frac{47}{36} + \frac{25x}{8} + \frac{3x^2}{8} - \left(\frac{11}{12} + \frac{x}{4} \right) y + \frac{y^2}{24} \\
&- \left(\frac{x^2}{2} y^{-2} + \left(\frac{x}{2} - 2x^2 \right) y^{-1} + \frac{1}{4} - \frac{3x}{4} + \frac{3x^2}{2} + \frac{y}{2} \right) \ln x + \left(x^2 y^{-2} + x(1-4x) y^{-1} + \frac{3x^2}{2} + y \right) \ln y \\
&+ \left(\frac{x^3}{6} y^{-3} - \frac{x^2(1+x)}{4} y^{-2} + \frac{x(1+3x)}{2} y^{-1} - \frac{23}{12} + \frac{9x}{4} - \frac{3x^2}{2} - \frac{y}{2} \right) \ln(1-y) \\
&+ \left(\frac{x^2}{6} y^{-2} - \frac{x}{4} \left(\frac{1}{3} + x \right) y^{-1} + \frac{5}{4} \left(\frac{1}{3} + x \right) + \frac{y}{2} \right) \frac{y-x}{y} \ln \frac{y-x}{y} \\
&\left. - \left(\frac{x^3}{6} y^{-3} + \frac{x^2(1-x)}{4} y^{-2} + \left(x - \frac{x^2}{2} \right) y^{-1} - \frac{2}{3} \right) \ln r_e \right], \tag{29}
\end{aligned}$$

$$x = \frac{m_\mu^2}{2m_e E_{\nu_\mu}}, \quad y = \frac{E_\mu}{E_{\nu_\mu}}, \quad r_e = \frac{m_e}{2E_{\nu_\mu}}. \tag{30}$$

Comparing the double-differential distribution in photon energy and muon energy in Ref. [31] to our numerical evaluation, we do not find agreement; in particular, the double-differential distribution in the calculation of Bardin and Dokuchaeva is not positive-definite in the kinematically allowed region of inverse muon decay. However, we reproduce the contribution to the muon energy spectrum from the events with photons above some energy cutoff in the limit $2m_e \Delta E \gg m_\mu^2$ for neutrino energies of modern accelerator experiments, not much larger than the threshold region in the inverse muon decay reaction.

At the fixed neutrino energy of 15 GeV, Fig. 1 shows muon energy spectra for the tree-level processes $\nu_\mu e^- \rightarrow \nu_e \mu^-$ and $\bar{\nu}_e e^- \rightarrow \bar{\nu}_\mu \mu^-$ as well as the $\mathcal{O}(\alpha)$ contribution to $\nu_\mu e^- \rightarrow \nu_e \mu^-$ from Eq. (29). We show the latter with an opposite sign for convenience. The radiative corrections reduce the cross section by 3–4%. They have the largest relative size for backward scattering and increase going to forward angles.

Integrating the muon energy spectrum over the kinematically allowed range in Eq. (5), we obtain the $\mathcal{O}(\alpha)$ contribution to the unpolarized inverse muon decay cross section σ . For illustration, we present two limits of interest. The leading term in m_e/E_ν expansion is given by

$$\begin{aligned}
\sigma \xrightarrow{r_e \ll 1} \sigma_{\text{LO}} &+ \frac{2G_{\text{F}}^2 m_e E_\nu \alpha}{\pi} \frac{\alpha}{\pi} \left[\frac{1}{24} \left(19 - 4\pi^2 \left(1 - \frac{3}{2}x + \frac{5}{2}x^2 \right) + 16 \ln r_e + 36x(1-2\ln x) + x^2(45-4x) \right) \right. \\
&+ \frac{x}{2} \left((1+3x) \text{Li}_2 x + (3-7x) \left(\text{Li}_2 \left(1 - \frac{1}{x} \right) + \frac{1}{2} \ln^2 x \right) - 8 + x \ln x \ln r_e \right) - x \ln x \left(1 - \frac{13}{4}x \right) \\
&\left. - \ln(1-x) \left(\left(1 - \frac{1}{2}x - \frac{5}{2}x^2 \right) \ln x + (1-x)^2(4 + \ln r_e) \right) - x \left(1 - \frac{x(3-x)}{6} \right) \ln r_e \right], \tag{31}
\end{aligned}$$

while the high-energy limit, $x \ll 1$, is described with

$$\sigma(E_\nu) - \sigma_{\text{LO}}(E_\nu) \xrightarrow{x \ll 1} \frac{G_{\text{F}}^2 m_e E_\nu \alpha}{12\pi} \frac{\alpha}{\pi} (19 - 4\pi^2 + 16 \ln r_e + 36x(1-2\ln x)), \tag{32}$$

where the leading terms coincide with the well-known expression in Ref. [25].

We provide the total cross section, double-differential distribution in muon energy and muon scattering angle, double-differential distribution in muon energy, and triple-differential distribution in muon energy, muon scattering angle, and photon energy in Appendices A, B and in Supplemental material.

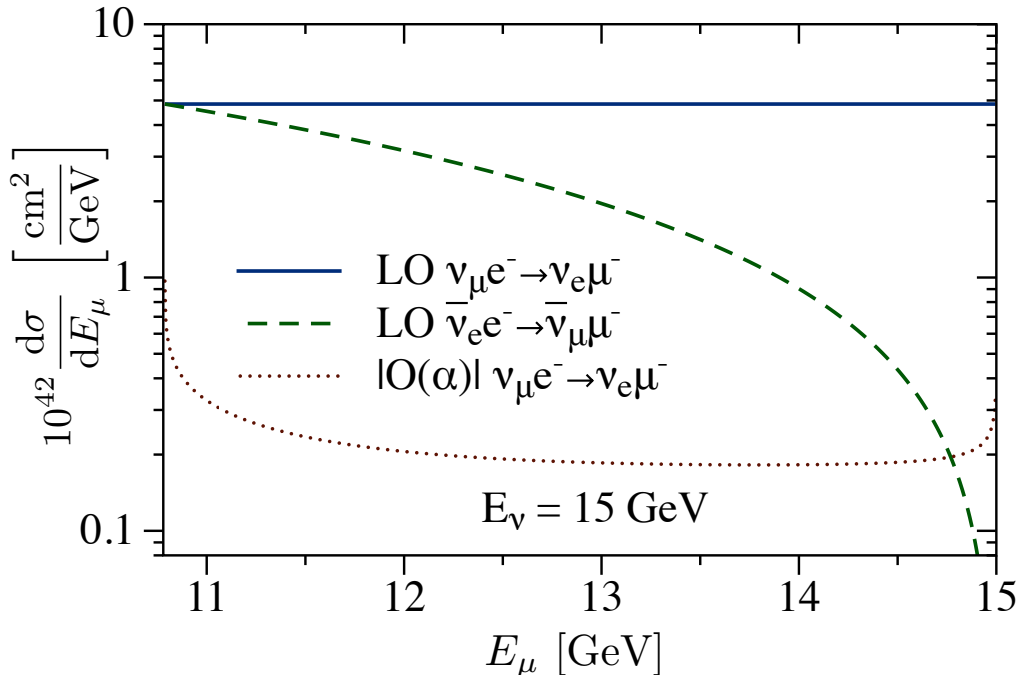


Figure 1: Leading-order muon spectrum and $O(\alpha)$ corrections for a fixed neutrino energy $E_\nu = 15$ GeV. The $\nu_\mu e^- \rightarrow \nu_e \mu^-$ process at leading order is shown by the blue solid line, and is compared to the spectrum in $\bar{\nu}_e e^- \rightarrow \bar{\nu}_\mu \mu^-$ at leading order, which is shown by green dashed line, and to the $O(\alpha)$ contribution in Eq. (29), cf. the red dotted line. The $O(\alpha)$ contribution is negative, i.e., decreases the total and differential cross sections at all values of muon energy.

6 Distortion of experimentally-accessed distributions

Experimentally, inverse muon decay events are distinguished from other reactions by looking for high-energy muons, above the E_μ^{\min} of Eq. (23) with no other particles in the final state, and which are along the direction of the incoming neutrino due to the kinematics of elastic scattering from electrons. Radiative corrections cause events with real photons in the final state and with a different distribution of muon energies and angles than in the tree-level process. This section explores those changes from the tree-level predictions.

Experiments will need to reject events from ν_μ quasielastic scattering on nucleons in nuclei which may appear to be consistent with elastic kinematics, but which will have a recoiling proton in the final state. Similarly, inelastic processes can produce high-energy forward muons with other particles in the final state. Because there are many possible elastic and inelastic reactions, a common experimental strategy is to remove events with any other visible energy than the muon in the final state. An energetic real photon from radiative processes, even one nearly collinear with the muon, may produce visible energy that will veto the event due to this requirement.

While this experimental strategy will be common to all measurements, the details of the effect will be particular to each experimental setup. In its analysis [5], MINERvA predicted the relative acceptance as a function of photon energy, and that prediction is shown in Fig. 2.

Averaging over high-energy tails of the expected flux in the DUNE experiment [49] and medium-energy “neutrino” (forward horn current) mode for the MINERvA experiment [2, 3, 50], we provide the effect of $O(\alpha)$ on muon energy spectra for two representative examples of neutrino experiments that do or will use IMD to constrain its high-energy flux tails in Figs. 3. For MINERvA and DUNE predictions, we average over the (anti)neutrino energy above the threshold value E_ν^{thr} but below 30 and 80 GeV respectively. We

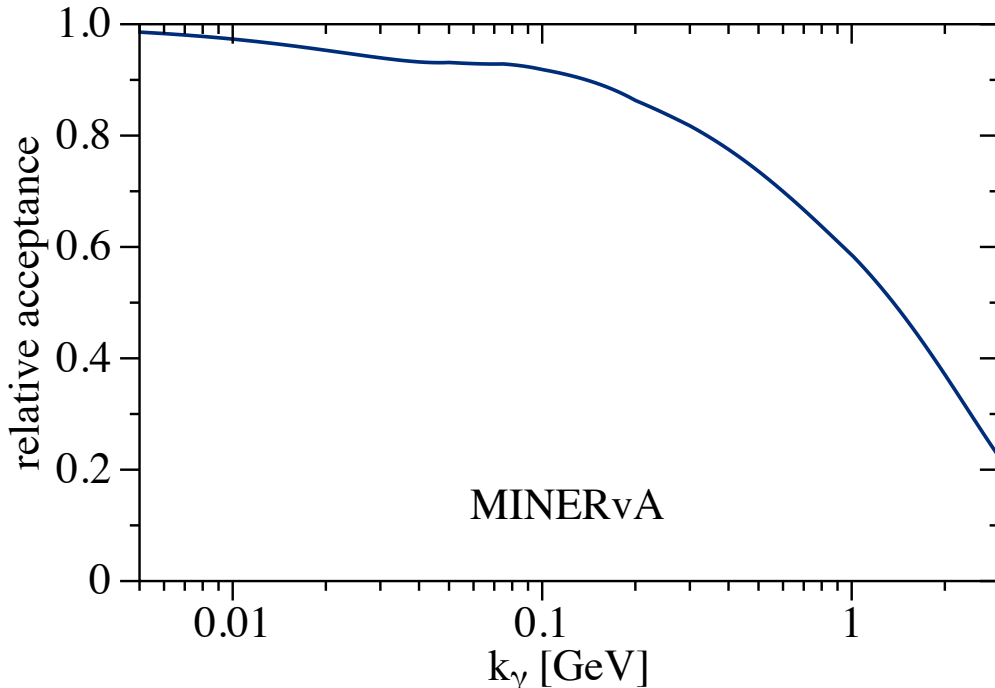


Figure 2: MINERvA’s probability to accept a radiative IMD event as a function of collinear photon energy.

illustrate this averaging on the left panel of Fig. 3 and compare it to fluxes averaged over the same region in both experiment. The average over the flux decreases the resulting cross section compared to the fixed energy $E_\nu = 15$ GeV result shown in Fig. 1, since the monotonically falling with (anti)neutrino energy flux is convoluted with slower rising cross sections. Distortions of the muon energy spectrum increase as the neutrino energy approaches the threshold of the inverse muon decay from above.

The effect on the measurable cross section from the removal of some events with real photons is also shown in Fig. 3 for comparison with the $O(\alpha)$ correction, and it is less than a 1% reduction in the observed rate, with a larger effect for higher muon energies.

The kinematics of elastic scattering from electrons produces a relationship between the muon energy and angle with respect to the incoming neutrino direction. A useful combination is

$$\mathcal{F}(E_\mu, \theta_\mu) \equiv E_\mu \theta_\mu^2 \approx \left(1 - \frac{E_\mu}{E_\nu}\right) \left(2m_e - \frac{m_\mu^2}{E_\mu}\right). \quad (33)$$

When $E_\nu \gg E_\mu$ and $E_\mu \gg E_\mu^{\min}$, \mathcal{F} can approach its upper limit of $2m_e$.

In measurements of elastic neutrino-electron scattering by the MINERvA experiment [1, 3, 4], the same quantity was used to select events that were due to elastic scattering from electrons. In this case $E_e \gg E_e^{\min}$ for all of the selected events. However, for IMD for the experimental fluxes considered above from DUNE and MINERvA, neither condition above is true for most events, and therefore typically $\mathcal{F} \ll 2m_e$. In particular because the factor $\left(1 - \frac{E_\mu}{E_\nu}\right)$ is usually small, one might want to consider an “idealized” version of \mathcal{F} ,

$$\mathcal{F}^{\text{ideal}}(E_\mu, \theta_\mu) \equiv \frac{E_\mu \theta_\mu^2}{1 - \frac{E_\mu}{E_\nu}} \approx \left(2m_e - \frac{m_\mu^2}{E_\mu}\right). \quad (34)$$

However, this quantity is not accessible since the neutrino energy is not known on an event-by-event basis.

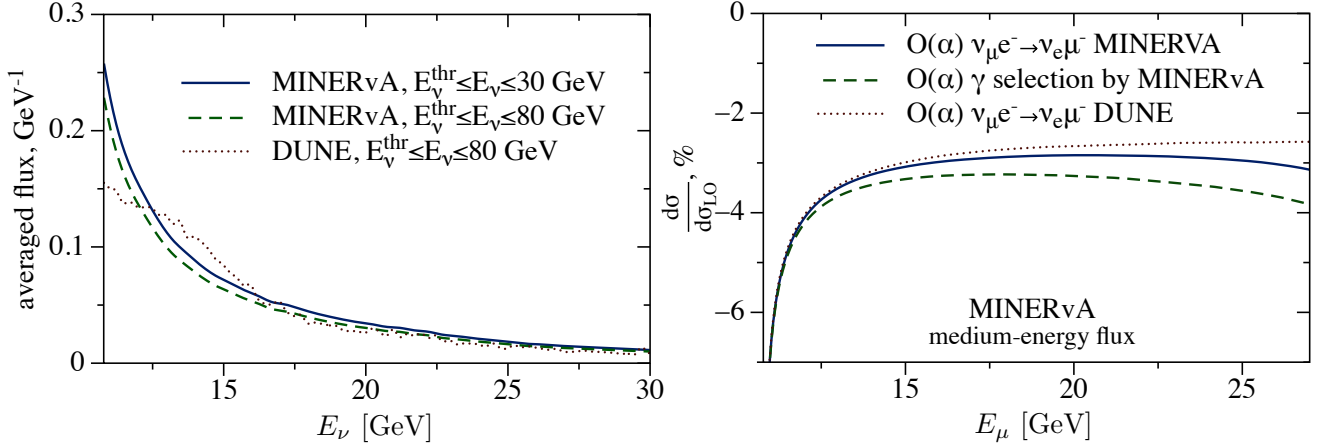


Figure 3: Left panel: DUNE and MINERvA medium-energy fluxes are averaged over the energies above the IMD threshold to 30 and 80 GeV respectively. For MINERvA experiment, we also present the averaging over the range up to 80 GeV. Right panel: Ratio of $O(\alpha)$ contribution to the leading-order result for the muon energy spectrum above E_{μ}^{\min} , averaged over the anticipated DUNE flux, shown by the red dashed line, is compared to this ratio averaged over the medium-energy flux of the MINERvA experiment, shown by the blue solid line. The green dashed line shows the further reduction in cross section due to the probability of vetoing the event due to the presence of a real radiated photon in MINERvA’s analysis of IMD events [5] MINERvA’s probability to accept events with real photons as a function of photon energy is shown in Figure 2.

In the measurement by the MINERvA experiment [5], the analysis enforced elastic kinematics for a “maximum” energy of likely candidate events in its beam. The variable $\mathcal{F}^{\text{MINERvA}}$,

$$\mathcal{F}^{\text{MINERvA}}(E_{\mu}, \theta_{\mu}) \equiv \frac{E_{\mu}\theta_{\mu}^2}{1 - \frac{E_{\mu}}{E^{\max}}}, \quad (35)$$

with $E^{\max} = 35$ GeV, was used for the selection of signal events by placing a cut on $\mathcal{F}^{\text{MINERvA}}(E_{\mu}, \theta_{\mu})$.

To illustrate various definitions for the variable \mathcal{F} , we present all three variants as a function of the final-state muon energy E_{μ} for the fixed neutrino energy $E_{\nu} = 15$ GeV in Fig. 4. The size of this variable in the inverse muon decay is below 10 – 100 keV. \mathcal{F} vanishes both in forward and backward directions for definitions in Eqs. (33) and (35) contrary to the forward scattering only for the definition in Eq. (34). In Fig. 5, we also present the tree-level distributions of the variable \mathcal{F} for the same neutrino energy in the region, which is allowed kinematically for all three definitions. We observe a significant redistribution of events moving from one definition of the variable \mathcal{F} to another.

To illustrate the effect of radiative corrections on the distribution of the \mathcal{F} variables, we keep MINERvA’s definition in Eq. (35) for applications to MINERvA’s study [2, 50]. However for a general experiment, including the application to the DUNE flux [49] in this paper, we don’t wish to enforce a maximum neutrino energy above which we would drop the constraint, so we study instead the original \mathcal{F} of Eq. (33). We present in Fig. 6 the distribution of the variable $\mathcal{F}^{\text{MINERvA}}$ at tree level, and compare it to the $O(\alpha)$ contribution of radiative corrections by integrating the double-differential distribution in muon energy and muon scattering angle, and by providing the naive estimate assuming the kinematics of the radiation-free process and Eq. (29). $O(\alpha)$ contributions shift the distribution of $\mathcal{F}^{\text{MINERvA}}$ variable by a percent-level correction. Note also that all inverse muon decay events from neutrinos of energy $E_{\nu} \leq 30$ GeV belong to the first bin in the variable $\mathcal{F}^{\text{MINERvA}}$, i.e. $0 \leq \mathcal{F}^{\text{MINERvA}} \leq 250$ keV, with the current experimental resolution [5].

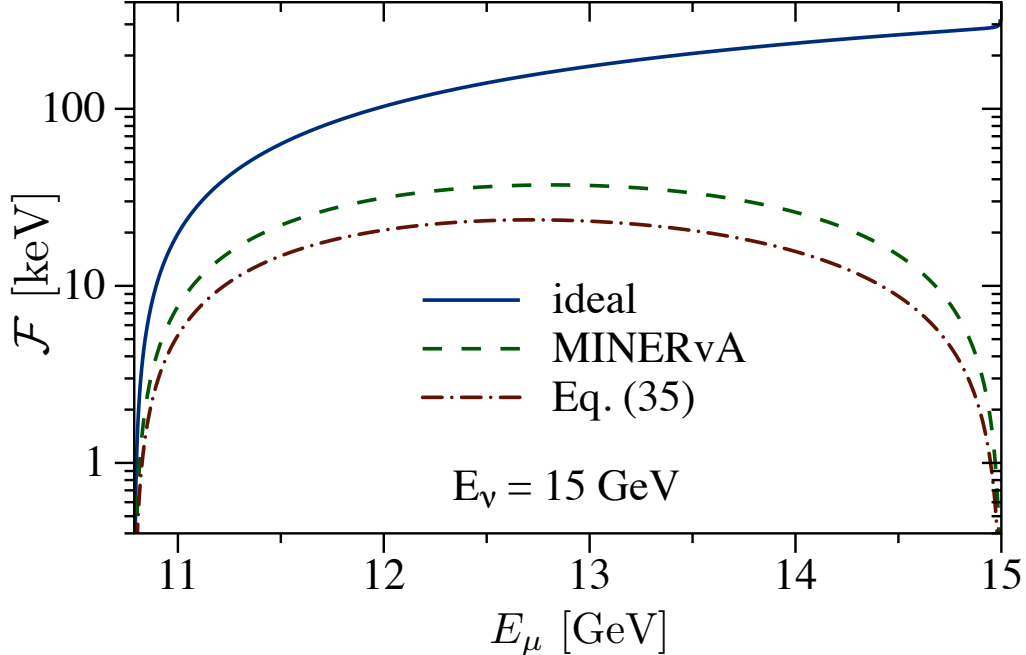


Figure 4: The variable \mathcal{F} as defined in Eqs. (33), (34), and (35) is presented as a function of the muon energy E_μ at the fixed neutrino energy $E_\nu = 15$ GeV .

7 Conclusions and Outlook

The goal of this paper is to enable percent-level constraints on the incoming (anti)neutrino fluxes by measuring the inverse muon decay reaction on the atomic electrons. Thus, we performed a study of radiative corrections and various cross sections in the inverse muon decay. We confirmed analytical expression for the muon energy spectrum and have provided triple-differential distribution in muon energy, muon scattering angle, and photon energy; double-differential distribution in muon energy and muon scattering angle; double-differential distribution in muon energy and photon energy, and total cross section. We investigated the effects of $O(\alpha)$ radiative corrections on the muon energy spectrum and experimentally-accessed distribution of the variable \mathcal{F} . In both cases, the corresponding distortions have the percent-level size.

We have clarified the definition for the experimentally-accessed variable \mathcal{F} . Inverse muon decay events contribute to the lowest bins of the variable \mathcal{F} . The size of this variable in the inverse muon decay is much smaller than in the elastic (anti)neutrino-electron scattering. The \mathcal{F} distribution provides a reasonable discriminant of keV to tens of keV size for (anti)neutrino energies well below the parameter E_ν^{\max} .

Providing radiative corrections to the inverse muon decay paves the way for percent-level constraints of high-energy tails in incoming neutrino flux of modern and future neutrino oscillation and cross-section experiments.

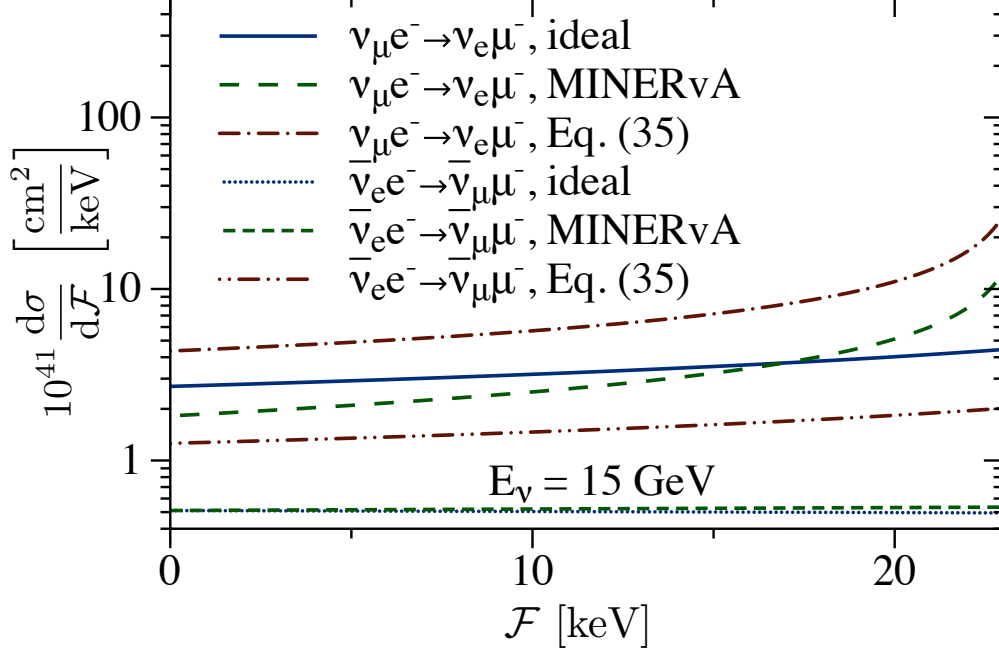


Figure 5: Distribution of the variable \mathcal{F} for the tree-level events in IMD reaction according to definitions in Eqs. (33), (34), and (35) is shown at the fixed neutrino energy $E_\nu = 15$ GeV.

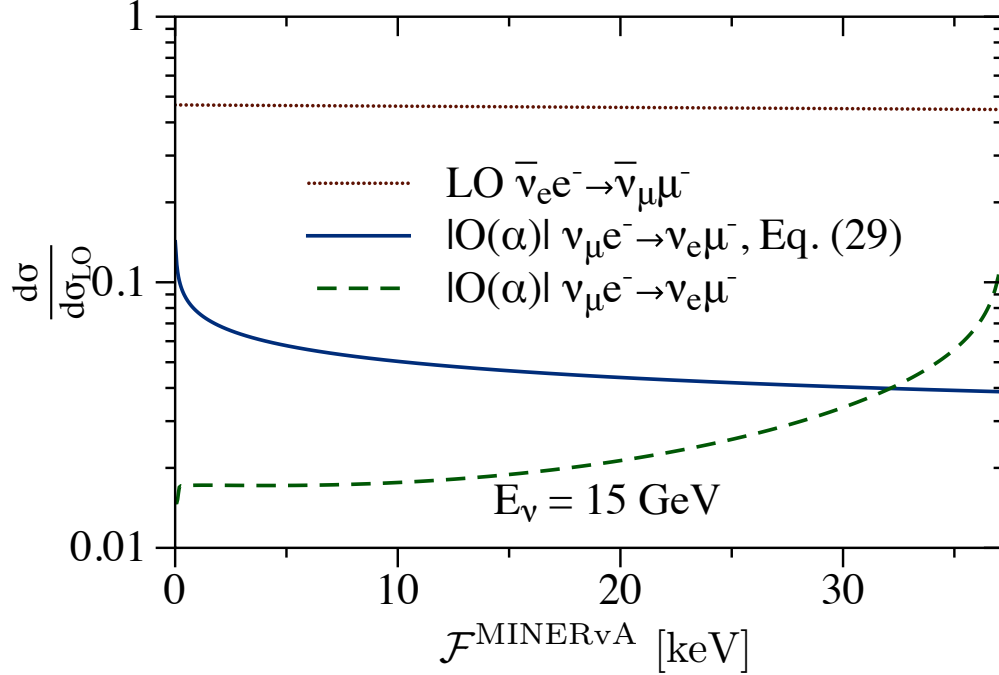


Figure 6: Comparisons of leading order and $O(\alpha)$ correction in the distribution of the variable $\mathcal{F}^{\text{MINERvA}}$ for a fixed neutrino energy $E_\nu = 15$ GeV. The ratio of the leading-order processes, $\nu_\mu e^- \rightarrow \nu_e \mu^-$ to $\bar{\nu}_e e^- \rightarrow \bar{\nu}_\mu \mu^-$ is almost constant, as it is shown by the red dotted line. The $O(\alpha)$ correction from Eq. (29) is shown by the blue solid line under the assumption that the kinematics are identical to that of radiation-free scattering. It is compared to the “true” $O(\alpha)$ contribution, which is obtained by integrating the appropriate double-differential distribution and adding virtual and soft-photon corrections. Note that both $O(\alpha)$ contributions are negative, and so decrease the cross section.

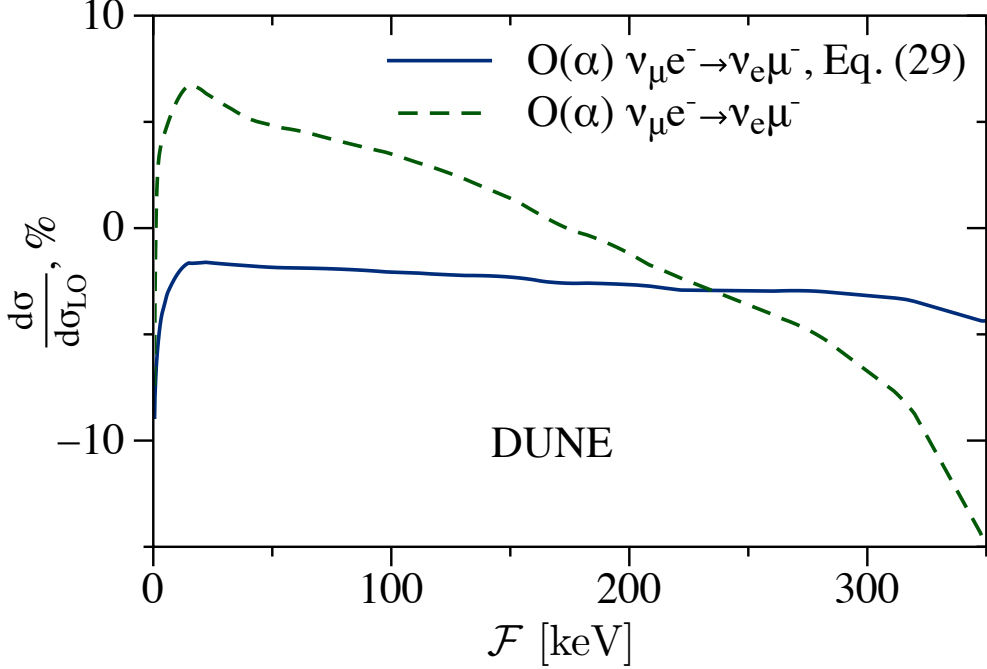


Figure 7: Ratios of the $O(\alpha)$ contribution to the leading-order result for the distribution of the variable \mathcal{F} , cf. Eq. (33), averaged over the anticipated DUNE flux. The $O(\alpha)$ correction in Eq. (29), assuming the kinematics of radiation-free scattering, the blue solid line, is compared to the $O(\alpha)$ contribution, which is obtained by integrating the appropriate double-differential distribution and adding virtual and soft-photon corrections on top, cf. the green dashed line.

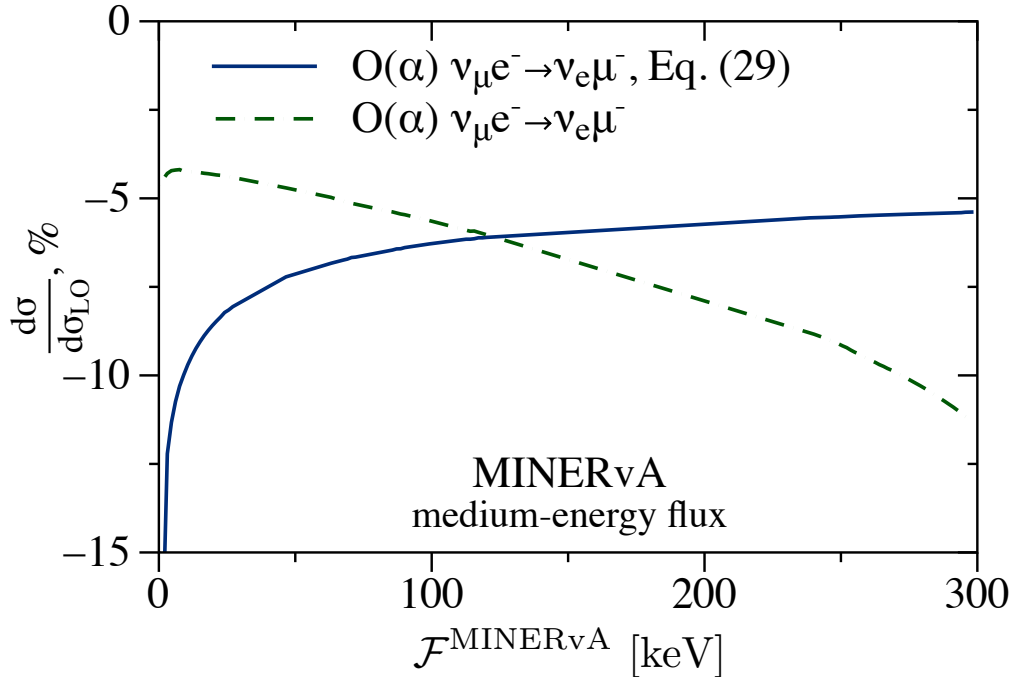


Figure 8: Same as Fig. 7 but for the medium-energy flux of the MINERvA experiment according to the definition of the variable $\mathcal{F}^{\text{MINERvA}}$ in Eq. (35).

Acknowledgments

O.T. thanks Matthias Heller and Marc Vanderhaeghen for technical discussions while working on other projects. This work is supported by the US Department of Energy through the Los Alamos National Laboratory and by LANL's Laboratory Directed Research and Development (LDRD/PRD) program under project number 20210968PRD4. Los Alamos National Laboratory is operated by Triad National Security, LLC, for the National Nuclear Security Administration of U.S. Department of Energy (Contract No. 89233218CNA000001). This work was also supported by the U.S. Department of Energy, Office of Science, Office of High Energy Physics, under Awards DE-SC0019095 and DE-SC0008475. KSM acknowledges support from a Fermilab Intensity Frontier Fellowship during the early stages of this work, and from the University of Rochester's Steven Chu Professorship in Physics. DR gratefully acknowledges support from a Cottrell Postdoctoral Fellowship, Research Corporation for Scientific Advancement award number 27467 and National Science Foundation Award CHE2039044. FeynCalc [51, 52], LoopTools [53], Mathematica [54] and DataGraph were extremely useful in this work.

A Triple-differential distribution

In Appendix, we provide analytic expressions for a few unpolarized cross sections of interest. The triple-differential cross section with respect to the muon angle, muon energy, and photon energy is given by:

$$\frac{d\sigma}{dE_\mu df dk_\gamma} = \frac{G_F^2}{2\pi m_e E_\nu^2} \frac{\alpha}{\pi} \text{I}, \quad (36)$$

$$\begin{aligned} \text{I} = & \frac{\rho f^2 (k_\gamma + E_\mu) (l^2)^2 + (k_\gamma (s + m_\mu^2) - E_\mu l^2) (2s - m_\mu^2 - m_e^2) + 4E_\mu E_\nu m_e (s - m_\mu^2) - 2k_\gamma s l^2}{k_\gamma \sqrt{d}} \\ & - \frac{2\rho^2 m_\mu^2 m_e (s - m_\mu^2) E_\nu f^4 \sigma}{d^{3/2}} - \frac{3}{16} \frac{m_e + k_\gamma}{m_e} \frac{\sigma^2}{\rho^2 f^4 k_\gamma^2} + \frac{m_e + k_\gamma}{m_e} \frac{(E_\mu^2 + k_\gamma^2 + 4m_e k_\gamma) (l^2)^2}{4f^2 k_\gamma^2} - \frac{2m_e^2 E_\nu^2 l_0^2}{f^2 k_\gamma^2} \\ & - \frac{m_e + k_\gamma}{m_e} \frac{(l^2 - k_\gamma^2 - 2l_0 k_\gamma) (m_\mu^2 + m_e^2)^2}{4f^2 k_\gamma^2} + \frac{2m_e E_\nu (m_e + E_\nu) l_0 l^2}{f^2 k_\gamma^2} + \frac{(2l^2 - 4E_\nu l_0 + l_0^2) (m_\mu^2 - m_e^2)}{f^2} \\ & - \frac{m_e + k_\gamma}{m_e} \frac{(m_\mu^2 - m_e^2 - 2m_e (l_0 - 3(m_e + E_\nu))) l^2 - 2(E_\nu^2 + 2E_\nu l_0 - m_\mu^2) m_e^2}{2f^2} - \frac{(E_\nu^2 - 4m_e l_0) l^2}{f^2} \\ & - \frac{(m_e (9l^2 - 4m_\mu^2) - 4l_0 (m_\mu^2 + 2m_e^2)) l^2}{4f^2 k_\gamma^2} + \frac{(l_0 - 2k_\gamma) (l_0 - 2m_e - 2E_\nu) (l^2)^2}{2f^2 k_\gamma^2} - \frac{m_e^2 (l^2 - 4m_\mu^2) l^2}{4f^2 k_\gamma^2} \\ & - \frac{\left((l^2)^2 + E_\nu (l_0 - m_e - k_\gamma) l^2 + 2(l_0 + E_\nu) k_\gamma^3 + 2l_0^3 k_\gamma \right) (m_\mu^2 - m_e^2)}{2f^2 k_\gamma^2} - \frac{E_\nu (l^2 + k_\gamma l_0) l^2}{f^2 k_\gamma} \\ & - \frac{m_e ((l_0 - k_\gamma) (l^2 - 4k_\gamma l_0) + (2k_\gamma^2 + 6k_\gamma l_0 - 2l_0^2) E_\nu) (m_\mu^2 - m_e^2)}{2f^2 k_\gamma^2} - \frac{l_0 (l_0^2 l^2 + 2m_\mu^2 m_e^2)}{f^2 k_\gamma} \\ & + \frac{k_\gamma ((l_0^2 - m_\mu^2 - 5k_\gamma (l_0 - E_\nu) - 2(E_\nu - k_\gamma) l_0) l^2 - (E_\nu l_0 - k_\gamma (2l_0 + 3E_\nu)) m_\mu^2) l^2}{m_e 2f^2 k_\gamma^2} \\ & + \frac{(2E_\nu l_0 (3l^2 - 8m_e l_0 + 4m_e^2) + 4l_0^2 (m_\mu^2 + 2m_e l_0 - 5m_e^2) + l^2 (2m_\mu^2 + 7m_e l_0)) E_\nu}{2f^2 k_\gamma^2} \\ & - \frac{12E_\nu (E_\mu l^2 + m_e l_0 (l_0 - E_\nu)) + 4m_e l_0 (m_e l_0 + m_\mu^2) + m_e E_\nu (3l^2 - 4m_e l_0)}{2f^2}, \quad (37) \end{aligned}$$

with the kinematic notations

$$\sigma = \rho (E_\nu^2 - f^2 - E_\mu^2 + m_\mu^2) (l^2 - 2k_\gamma l_0) + 4k_\gamma m_\mu f^2, \quad (38)$$

$$d = \beta^2 m_\mu^2 l^2 E_\nu^2 (l^2 + 4k_\gamma^2 - 4k_\gamma l_0) \sin^2 \theta_\mu + \frac{\sigma^2}{4}, \quad (39)$$

and the squared energy in the center-of-mass reference frame $s = m_e^2 + 2m_e E_\nu$.

B Double-differential distribution in muon energy and muon angle

Integrating Eq. (36) over the photon energy k_γ , we obtain the double-differential cross section with respect to the recoil muon energy and muon angle. The result is expressed in a similar to elastic neutrino-electron scattering form [10]:

$$\frac{d\sigma}{dE_\mu df} = \frac{G_F^2}{\pi} \frac{m_\mu}{E_\nu^2} \frac{\alpha}{m_e} \frac{1}{\pi} \left(a + b \frac{f}{l_0^2 - f^2} \ln \frac{1 + \beta}{1 - \beta} + c \ln \frac{l_0 + f}{l_0 - f} + df \ln \frac{l_0 - \beta f \cos \delta - \sqrt{g}}{l_0 - \beta f \cos \delta + \sqrt{g}} \right), \quad (40)$$

with $g = (f \cos \delta - \beta l_0)^2 + \rho^2 f^2 \sin^2 \delta$ and the angle δ between vectors \vec{f} and \vec{p}_μ :

$$\cos \delta = \frac{E_\nu^2 - \beta^2 E_\mu^2 - f^2}{2\beta E_\mu f}. \quad (41)$$

The coefficients a , b , c , and d are given by

$$\begin{aligned} a = & \frac{\beta \cos \delta}{\rho} (m_\mu^2 - m_e^2) + \frac{f}{m_\mu} \left(s - m_\mu^2 - m_e^2 - \frac{2(s - m_\mu^2)(s - m_e^2)}{l^2} \right) + \left(f + \frac{10m_\mu \beta \cos \delta}{\rho} \right) \frac{l_0 - \beta f \cos \delta}{2\rho} \\ & + \left(1 - \frac{l_0}{4m_e} \right) \frac{m_\mu}{f} \frac{\beta^2}{\rho^2} (1 - 3 \cos^2 \delta) l^2 + \frac{m_\mu^2 + m_e^2}{m_e} \frac{f - \beta l_0 \cos \delta}{2\rho} - \frac{m_\mu}{m_e} \frac{\beta \cos \delta}{\rho} \frac{2l_0^2 + f^2}{\rho} \\ & + \frac{3l_0 f}{2} \frac{m_\mu}{m_e} \frac{1 + \beta^2 \cos^2 \delta}{\rho^2}, \end{aligned} \quad (42)$$

$$b = \frac{2m_\mu l_0^2}{\beta \rho^2} + \frac{m_e E_\nu}{\beta m_\mu} (s - m_\mu^2) + \frac{m_\mu^2 - m_e^2}{\beta} \frac{l_0 - \beta f \cos \delta}{\rho} - 4m_\mu f \frac{l_0 - \frac{1}{2}\beta f \cos \delta}{\rho} \frac{\cos \delta}{\rho}, \quad (43)$$

$$\begin{aligned} c = & \frac{m_\mu}{2} \left(l_0 + \frac{m_\mu}{\rho} \right) - \frac{s^2 + m_e^3 E_\nu}{2m_\mu m_e} - \left(1 + \frac{2\beta \cos \delta}{\rho} \frac{m_\mu}{f} - \frac{m_\mu^2}{f^2} \frac{\beta^2}{\rho^2} \frac{1 - 3 \cos^2 \delta}{2} \right) \frac{l^2 (l^2 - 4m_e l_0)}{4m_\mu m_e} \\ & + \left(1 + \frac{\beta \cos \delta}{\rho} \frac{m_\mu}{f} \right) \left(\frac{1}{\rho} - \frac{m_\mu^2 + m_e^2}{4m_\mu m_e} \right) l^2 - \frac{\beta \cos \delta}{2\rho} \left(\frac{m_\mu}{f} \frac{l^2}{\rho} + \frac{l_0 (2s - m_\mu^2 - m_e^2)}{f} \right), \end{aligned} \quad (44)$$

$$d = \frac{\sqrt{g}}{\rho} + \frac{\rho}{\sqrt{g}} \left(s - m_\mu^2 + \frac{m_e E_\nu}{2m_\mu^2} (s + m_\mu^2) - m_\mu \frac{l_0 - \beta f \cos \delta}{\rho} \right). \quad (45)$$

References

- [1] J. Park *et al.* (MINERvA), *Phys. Rev. D* **93**, 112007 (2016), [arXiv:1512.07699 \[physics.ins-det\]](#).
- [2] L. Aliaga *et al.* (MINERvA), *Phys. Rev. D* **94**, 092005 (2016), [Addendum: *Phys. Rev. D* **95**, 039903 (2017)], [arXiv:1607.00704 \[hep-ex\]](#).
- [3] E. Valencia *et al.* (MINERvA), *Phys. Rev. D* **100**, 092001 (2019), [arXiv:1906.00111 \[hep-ex\]](#).
- [4] L. Zazueta *et al.* (MINERvA), (2022), [arXiv:2209.05540 \[hep-ex\]](#).

- [5] D. Ruterbories *et al.* (MINERvA), *Phys. Rev. D* **104**, 092010 (2021), [arXiv:2107.01059 \[hep-ex\]](#).
- [6] C. M. Marshall, K. S. McFarland, and C. Wilkinson, *Phys. Rev. D* **101**, 032002 (2020), [arXiv:1910.10996 \[hep-ex\]](#).
- [7] B. Abi *et al.* (DUNE), (2020), [arXiv:2002.03005 \[hep-ex\]](#).
- [8] O. Tomalak, Q. Chen, R. J. Hill, and K. S. McFarland, *Nature Commun.* **13**, 5286 (2022), [arXiv:2105.07939 \[hep-ph\]](#).
- [9] O. Tomalak, Q. Chen, R. J. Hill, K. S. McFarland, and C. Wret, *Phys. Rev. D* **106**, 093006 (2022), [arXiv:2204.11379 \[hep-ph\]](#).
- [10] O. Tomalak and R. J. Hill, *Phys. Rev. D* **101**, 033006 (2020), [arXiv:1907.03379 \[hep-ph\]](#).
- [11] M. Ram, *Phys. Rev.* **155**, 1539 (1967).
- [12] S. Weinberg, *Phys. Rev. Lett.* **19**, 1264 (1967).
- [13] G. 't Hooft, *Phys. Lett. B* **37**, 195 (1971).
- [14] S. Sarantakos, A. Sirlin, and W. J. Marciano, *Nucl. Phys. B* **217**, 84 (1983).
- [15] J. N. Bahcall, M. Kamionkowski, and A. Sirlin, *Phys. Rev. D* **51**, 6146 (1995), [arXiv:astro-ph/9502003](#).
- [16] D. Y. Bardin and V. A. Dokuchaeva, *Nucl. Phys. B* **246**, 221 (1984).
- [17] D. Y. Bardin and V. A. Dokuchaeva, *Sov. J. Nucl. Phys.* **43**, 975 (1986).
- [18] M. Passera, *Phys. Rev. D* **64**, 113002 (2001), [arXiv:hep-ph/0011190](#).
- [19] M. Green, *J. Phys. G* **7**, 1169 (1981).
- [20] D. Y. Bardin and V. A. Dokuchaeva, *Sov. J. Nucl. Phys.* **39**, 563 (1984).
- [21] E. D. Zhizhin, R. V. Konoplich, and Y. P. Nikitin, *Izv. Vuz. Fiz.* **1975**, 82 (1975).
- [22] N. Byers, R. Ruckl, and A. Yano, *Physica A* **96**, 163 (1979).
- [23] P. Salomonson and Y. Ueda, *Phys. Rev. D* **11**, 2606 (1975).
- [24] M. Green and M. J. G. Veltman, *Nucl. Phys. B* **169**, 137 (1980), [Erratum: *Nucl. Phys. B* 175, 547 (1980)].
- [25] W. J. Marciano and A. Sirlin, *Phys. Rev. D* **22**, 2695 (1980), [Erratum: *Phys. Rev. D* 31, 213 (1985)].
- [26] K.-i. Aoki, Z. Hioki, R. Kawabe, M. Konuma, and T. Muta, *Prog. Theor. Phys.* **65**, 1001 (1981).
- [27] K.-i. Aoki and Z. Hioki, *Prog. Theor. Phys.* **66**, 2234 (1981).
- [28] Z. Hioki, *Prog. Theor. Phys.* **67**, 1165 (1982).
- [29] W. J. Marciano and Z. Parsa, *J. Phys. G* **29**, 2629 (2003), [arXiv:hep-ph/0403168](#).
- [30] A. Sirlin and A. Ferroglia, *Rev. Mod. Phys.* **85**, 263 (2013), [arXiv:1210.5296 \[hep-ph\]](#).
- [31] D. Y. Bardin and V. A. Dokuchaeva, *Nucl. Phys. B* **287**, 839 (1987).
- [32] D. Geiregat *et al.* (CHARM-II), *Phys. Lett. B* **247**, 131 (1990).

- [33] P. Vilain *et al.* (CHARM-II), *Phys. Lett. B* **364**, 121 (1995).
- [34] O. Tomalak, *Phys. Lett. B* **829**, 137108 (2022), arXiv:2112.12395 [hep-ph].
- [35] O. Tomalak, Q. Chen, R. J. Hill, and K. S. McFarland, *Nature Commun.* **13**, 5286 (2022).
- [36] E. Fermi, *Z. Phys.* **88**, 161 (1934).
- [37] R. P. Feynman and M. Gell-Mann, *Phys. Rev.* **109**, 193 (1958).
- [38] H. Arason, D. J. Castano, B. Keszthelyi, S. Mikaelian, E. J. Piard, P. Ramond, and B. D. Wright, *Phys. Rev. D* **46**, 3945 (1992).
- [39] F. Antonelli and L. Maiani, *Nucl. Phys. B* **186**, 269 (1981).
- [40] R. J. Hill and O. Tomalak, *Phys. Lett. B* **805**, 135466 (2020), arXiv:1911.01493 [hep-ph].
- [41] M. Vanderhaeghen, J. M. Friedrich, D. Lhuillier, D. Marchand, L. Van Hoorebeke, and J. Van de Wiele, *Phys. Rev. C* **62**, 025501 (2000), arXiv:hep-ph/0001100.
- [42] M. Heller, O. Tomalak, and M. Vanderhaeghen, *Phys. Rev. D* **97**, 076012 (2018), arXiv:1802.07174 [hep-ph].
- [43] M. Heller, O. Tomalak, M. Vanderhaeghen, and S. Wu, *Phys. Rev. D* **100**, 076013 (2019), arXiv:1906.02706 [hep-ph].
- [44] T. D. Lee and A. Sirlin, *Rev. Mod. Phys.* **36**, 666 (1964).
- [45] F. Bloch and A. Nordsieck, *Phys. Rev.* **52**, 54 (1937).
- [46] N. Nakanishi, *Prog. Theor. Phys.* **19**, 159 (1958).
- [47] T. Kinoshita, *J. Math. Phys.* **3**, 650 (1962).
- [48] T. D. Lee and M. Nauenberg, *Phys. Rev.* **133**, B1549 (1964).
- [49] “Dune fluxes,” <http://home.fnal.gov/~ljf26/DUNEFluxes/> (2019).
- [50] J. Devan *et al.* (MINERvA), *Phys. Rev. D* **94**, 112007 (2016), arXiv:1610.04746 [hep-ex].
- [51] R. Mertig, M. Bohm, and A. Denner, *Comput. Phys. Commun.* **64**, 345 (1991).
- [52] V. Shtabovenko, R. Mertig, and F. Orellana, *Comput. Phys. Commun.* **207**, 432 (2016), arXiv:1601.01167 [hep-ph].
- [53] T. Hahn and M. Perez-Victoria, *Comput. Phys. Commun.* **118**, 153 (1999), arXiv:hep-ph/9807565.
- [54] W. R. Inc., “Mathematica, Version 12.2.0.0,” (2022), campaign, IL, 2022.